Applied Electromagnetics III

Classical and IT based Modeling of the Magnetization Dynamics

Yoshifuru Saito[1], Hisashi Endo[1], Seiji Hayano[1] and Kenzo Miya[2]
([1]:Graduate School of Engineering, Hosei University, Tokyo 184-8584, Japan)
([2]: International Institute of Universality, Tokyo 113-0031, Japan)

Abstract. This paper reviews the classical magneitization models for computational use and proposes information technology (IT, in short) based model for the magnetodynamics in ferromagnetic materials. At first, Fourier model of the hysteretic magnetization is derived. Second, assuming the bar-like domain walls derives a domain-based model. A simple example verifies this validity of domain-based model. Third, a composite model by combining the Preisach with domain-based models is derived as well as Rayleigh's law is derived. Finally, IT based model for magnetodynamics in ferromagnetic materials is introduced.

1. Introduction

Modeling of the ferromagnetic materials is of paramount importance for modern computational magneto-dynamics in order to carry out the practical magnetic device design. Fundamentally, the elements comprising the modern electronic as well as electrical devices are classified into two major categories. One is the active element such as silicon controlled rectifier and Power MOS FET. The other is the passive element such as resistance, capacitance and inductance. Even if the inductors are regarded as one of the linear elements in the undergraduate textbook, practically most of them exhibit a serious non-linearity, e.g., saturation and hysteretic properties.

In the present paper, at first, we derive a phenomenological magnetization model by means of Fourier series. Second, assuming the bar-like domain walls leads to a domain-based model. Third, a composite model by combining the Preisach with domain-based models is derived. Analytical solution of this composite model leads to the famous Lord Rayleigh's law. Finally, we propose the IT based magnetization model. This IT based model is derived from the scanning electron microscopic (SEM, in short) images of the ferromagnetic materials. Practically this IT based model is applied to grain oriented silicon steel sheet. We recover the magnetization characteristics at the normal, lancet and strained magnetic domains on the SEM image.

Thus, this paper suggests an implementation methodology of computer-aided magnetic device design fully taking into account the magnetization characteristics in ferromagnetic materials.

2. Modeling of Ferromagnetic Magnetization

2.1 Model by Fourier series

Consider the sinusoidal time t varying flux densities $\mathbf{B}$ having angular frequency ω,

$$\mathbf{B} = \mathbf{B}_m Sin(\omega t), \tag{1}$$

then, as shown in Figs.1(a) and 1(b), we have the distorted field intensities $\mathbf{H}$ in (2)

represented in terms of Fourier series.

$$\mathbf{H} = \sum_{n=1}^{\infty} \mathbf{H}_n \sin(n\omega t) + \sum_{n=1}^{\infty} \mathbf{H}_n \cos(n\omega t) \qquad (2)$$
$$= \mathbf{H}_o + \mathbf{H}_e ,$$

where $\mathbf{H}_o$ and $\mathbf{H}_e$ are the odd and even components of the distorted field **H**, respectively.

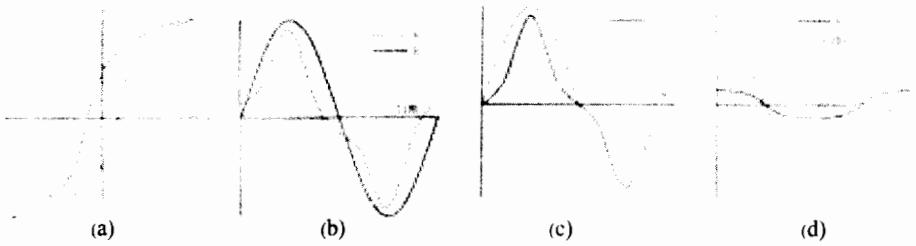

Fig.1. Typical hysteresis loop and time in phase components.

As shown in Figs. 1(c) and (d), the odd component $\mathbf{H}_o$ and even component $\mathbf{H}_e$, are, respectively, in phase with the flux density **B** and the time derivative $d\mathbf{B}/dt$. Thereby, a combination of $\mathbf{H}_o$ with **B** yields one of the saturation curves. Also, a combination of $\mathbf{H}_e$ with $d\mathbf{B}/dt$ yields a curve which represents the hysteretic property, because $\mathbf{H}_e(d\mathbf{B}/dt)$ provides the power loss per unit volume. Figs. 2(Left) and (Right) show the **B** vs. $\mathbf{H}_o$ and $d\mathbf{B}/dt$ vs. $\mathbf{H}_e$ curves, respectively. In the other words, by considering the relationship of Figs. 2(a) and (b), it is possible to derive a following Fourier based magnetization model (3).

$$\mathbf{H} = \mathbf{H}_0 + \mathbf{H}_e = \frac{1}{\mu}\mathbf{B} + \frac{1}{s}\frac{d\mathbf{B}}{dt} \qquad (3)$$

where μ, s are the permeability and hysteresis coefficient, respectively [1].

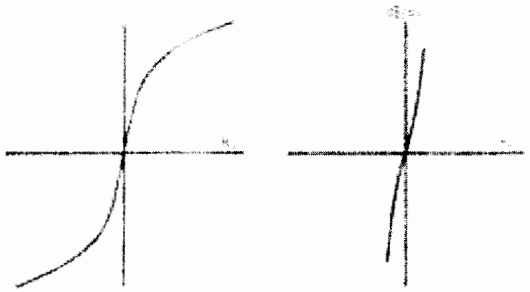

Fig.2. **B** vs $\mathbf{H}_0$ (Left) and $d\mathbf{B}/dt$ vs $\mathbf{H}_e$ (Right)

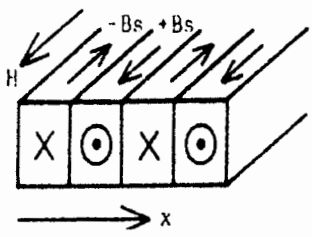

Fig.3. Bar-like magnetic

2.2 Domain-based Model

To derive a constitutive equation representing magnetization characteristics of ferromagnetic materials, let us consider a simple bar-like domain wall model shown in Fig.3. When an external magnetic field $\mathbf{H}_s$ is applied, (4) can be established.

$$\mathbf{B} = \mu_0 \mathbf{H}_s + n\mathbf{B}_s = \mu_0 \left(1 + \mathbf{H}_s^{-1}\mathbf{B}_s\right)\mathbf{H}_s = \mu \mathbf{H}_s \qquad (4)$$

where $\mathbf{B}_s$, n, μ_0 and μ are the saturation flux density in each of the domains, number of domains in accordance with the direction of $\mathbf{H}_s$, permeability of air, and permeability of the specimen, respectively. The constitutive equation should exhibit various magnetization characteristics, such as a hysteretic property. This means that the constitutive equation must be composed of parameters not affected by past histories. One of the unique properties independent of the past histories is an ideal or anhysteretic magnetization curve. If (4) has been established for the ideal magnetization curve, then obviously (4) represents a static magnetization characteristic corresponding to each of the domain situations. This means that the permeability μ in (4) can be obtained from the ideal magnetization curve.

Differentiation (4) with time t yields a following relation:

$$\frac{d\mathbf{B}}{dt} = \mu_0 \frac{d\mathbf{H}}{dt} + \mathbf{B}_s \frac{dn}{dt} = \left(\mu_0 + \mathbf{B}_s \frac{\partial n}{\partial \mathbf{H}} \right) \frac{d\mathbf{H}}{dt} + \mathbf{B}_s \frac{\partial n}{\partial x} \frac{dx}{dt} = \mu_r \frac{d\mathbf{H}}{dt} + \mathbf{B}_s \frac{\partial n}{\partial x} v \quad , \tag{5}$$

where $\mathbf{H}$, v, and μ_r are the applied field, velocity (dx/dt) of domain movement, and reversible permeability, respectively. Consideration of (5) suggests that the induced voltage per unit area ($d\mathbf{B}/dt$) is composed of the transformer and velocity induced voltages. When a hysteresis coefficient s (Ω/m) is introduced into (5), the magnetic field $\mathbf{H}_d$ due to the domain movement is given by

$$\mathbf{H}_d = \frac{1}{s} \mathbf{B}_s \frac{\partial n}{\partial x} v = \frac{1}{s} \left(\frac{d\mathbf{B}}{dt} - \mu_r \frac{d\mathbf{H}}{dt} \right) \quad , \tag{6}$$

where it has been assumed that the width of the domains is fixed and only their number changes as the specimen magnetized. Summation of the static field $\mathbf{H}_s$ in (4) and dynamic field $\mathbf{H}_d$ in (6) gives the domain-based magnetization model as [2]

$$\mathbf{H} = \mathbf{H}_s + \mathbf{H}_d = \frac{1}{\mu} \mathbf{B} + \frac{1}{s} \mathbf{B}_s \frac{\partial n}{\partial x} v = \frac{1}{\mu} \mathbf{B} + \frac{1}{s} \left(\frac{d\mathbf{B}}{dt} - \mu_r \frac{d\mathbf{H}}{dt} \right) \quad . \tag{7}$$

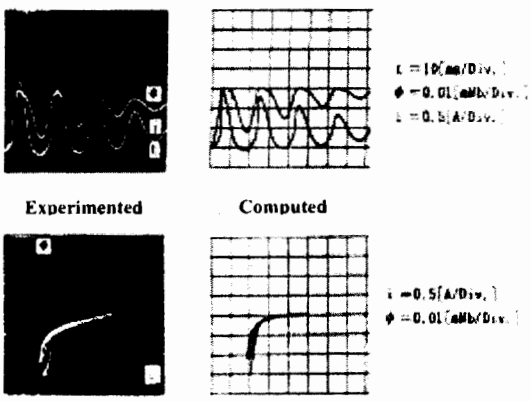

Fig.4. Experimented and computed results (K6A, TDK).

We had carried out intensive experimental verification of (7). Fig.4 shows one of the examples.

2.3 Preisach and Composite Models

According to Ref. [3], a reversing $\mathbf{H}_n$ and applied $\mathbf{H}_p$ field points are defined as shown in Fig. 5. By considering the trajectories in Fig.5, it is obvious that **B-H** trajectory takes different paths depending on the reversing field $\mathbf{H}_n$. Thereby, the flux density $\mathbf{B}$ is represented as a function of applied field $\mathbf{H}_p$ as well as reversing field $\mathbf{H}_n$:

$$\mathbf{B} = f(\mathbf{H}_p, \mathbf{H}_n) \quad . \tag{8}$$

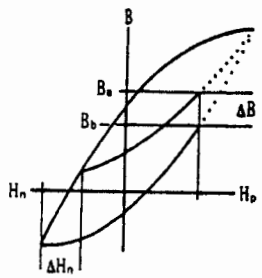

Fig.5. Derivation of Preisach model.

Moreover, consideration of a saturation flux density suggests that the **B-H** trajectories take different paths depending on the reversing fields $\mathbf{H}_n$, but always coincide at the saturation flux density. Thereby, rate of change $\partial \mathbf{B} / \partial \mathbf{H}_p$ with reversing field $\mathbf{H}_n$ takes non-zero value within the unsaturated region. This leads to the definition of the Preisach function Ψ as

$$\Psi = \frac{\partial^2 \mathbf{B}}{\partial \mathbf{H}_n \partial \mathbf{H}_p} \quad . \tag{9}$$

Application (5) to the magnetizing states shown in Fig. 5 gives

$$\mathbf{H}_p = \frac{1}{\mu}\mathbf{B}_a + \frac{1}{s}\left(\frac{\partial \mathbf{B}_a}{\partial t} - \mu_r \frac{\partial \mathbf{H}_p}{\partial t}\right) , \tag{10}$$

$$\mathbf{H}_p = \frac{1}{\mu}\mathbf{B}_a + \frac{1}{s}\left(\frac{\partial \mathbf{B}_a}{\partial t} - \mu_r \frac{\partial \mathbf{H}_p}{\partial t}\right) , \tag{11}$$

where the field $\Delta \mathbf{H}_n$ in Fig. 5 is so small that the parameters μ, μ_r, s are assumed to be constants.

Subtracting (10) from (11) yields

$$\frac{\Delta \mathbf{B}}{\mu} = \frac{\mathbf{B}_a - \mathbf{B}_b}{\mu} = \frac{1}{s}\left(\frac{\partial \mathbf{B}_a}{\partial t} - \frac{\partial \mathbf{B}_b}{\partial t}\right) = \frac{1}{s}\left(\frac{\partial \mathbf{B}_a}{\partial \mathbf{H}_p} - \frac{\partial \mathbf{B}_b}{\partial \mathbf{H}_p}\right)\frac{\partial \mathbf{H}_p}{\partial t} . \tag{12}$$

Rearrangement of (12) gives

$$\frac{s}{\partial \mathbf{H}_p / \partial t} = \frac{\mu}{\Delta \mathbf{B}}\left(\frac{\partial \mathbf{B}_b}{\partial \mathbf{H}_p} - \frac{\partial \mathbf{B}_a}{\partial \mathbf{H}_p}\right) . \tag{13}$$

In Fig. 4, if the limit of $\Delta \mathbf{H}_n$ goes to zero, then $\Delta \mathbf{B}/\mu$ is simultaneously to be zero. Thus, an assumption $\Delta \mathbf{H}_n = \Delta \mathbf{B}/\mu$ leads to

$$\lim_{\Delta \mathbf{H}_n \to 0} \frac{\mu}{\Delta \mathbf{B}}\left(\frac{\partial \mathbf{B}_b}{\partial \mathbf{H}_p} - \frac{\partial \mathbf{B}_a}{\partial \mathbf{H}_p}\right) = \frac{\partial^2 \mathbf{B}}{\partial \mathbf{H}_n \partial \mathbf{H}_p} . \tag{14}$$

From (9), (13) and (14), the hysteresis coefficient s in (6) is related to the Preisach function Ψ by

$$s = \Psi \frac{\partial \mathbf{H}}{\partial t} . \tag{15}$$

Substituting (15) into (6) after some modification (6) yields a following composite model:

$$\mathbf{H} + \frac{\mu_r}{\Psi} = \frac{1}{\mu}\mathbf{B} + \frac{1}{\Psi}\frac{d\mathbf{B}}{d\mathbf{H}} . \tag{16}$$

Let us consider that the parameters μ, μ_r, Ψ take the constants in the weakly magnetized region known as the Rayleigh region, then (16) gives

$$\mathbf{B} = \mu\left(\mathbf{H}_n + \mathbf{H}_p\right) + \frac{\mu^2}{\psi}\left(1 - \frac{\mu_r}{\mu}\right)\left(\varepsilon^{-\frac{\mu}{\psi}(\mathbf{H}_n + \mathbf{H}_p)} - 1\right) - \mathbf{B}_n \varepsilon^{-\frac{\mu}{\psi}(\mathbf{H}_n + \mathbf{H}_p)} , \tag{18}$$

where $\mathbf{H}_p$, $\mathbf{H}_n$ and $\mathbf{B}_n$ are the applied and reversing point fields and reversing point flux density, respectively. The fields $\mathbf{H}_p$ and $\mathbf{H}_n$ are so small that the following approximations could be held:

$$\varepsilon^{-\frac{\mu}{\psi}(\mathbf{H}_p + \mathbf{H}_n)} \approx 1 - \frac{\mu}{\psi}\left(\mathbf{H}_p + \mathbf{H}_n\right) + \frac{1}{2}\left[\frac{\mu}{\psi}\left(\mathbf{H}_p + \mathbf{H}_n\right)\right]^2 . \tag{19}$$

Substituting (19) into (18) and setting $\mathbf{H}_n = \mathbf{B}_n = 0$ yields

$$\mathbf{B} = \mu_r \mathbf{H}_p + \frac{1}{2}\psi \mathbf{H}_p^2\left(1 - \frac{\mu_r}{\mu}\right) \approx \mu_r \mathbf{H}_p + \frac{1}{2}\psi \mathbf{H}_p^2 , \tag{20}$$

where $\mu >> \mu_r$ has been assumed. (20) is obviously Rayleigh's initial magnetization curve [3]. Hence, it is revealed that the Preisach function Ψ corresponds to the Rayleigh's constant. Imposing symmetrical **B**-**H** loop condition to (16) yields the reversing flux density $\mathbf{B}_n$ as

$$\mathbf{B}_n = \mu\mathbf{H}_n + \left(\mu\mathbf{H}_n - \frac{\mu^2}{\psi} + \frac{\mu_r\mu}{\psi}\right)\tanh\left(\frac{\psi}{\mu}\mathbf{H}_n\right). \tag{21}$$

After employing the approximations as these of the derivation (20), substituting this into (18) yield a lower branch of Rayleigh loop:

$$\mathbf{B} = (\mu_r + \psi)\mathbf{H}_p + \frac{1}{2}\left(\mathbf{H}_p^2 - \mathbf{H}_n^2\right) . \tag{22}$$

Thus, the composite model (16) is including all of the Rayleigh's Law.

2.4 IT based Model

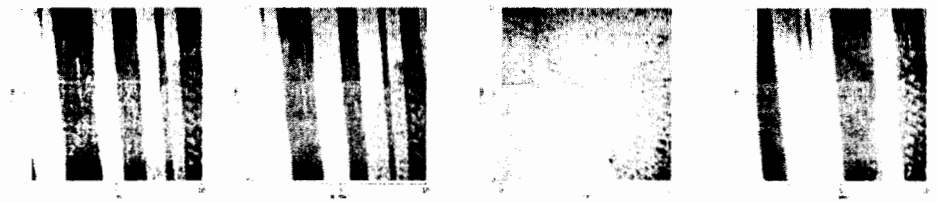

(a)**H**=0.0 A/m, **B**=0.0 T (b)**H**=2.9 A/m, **B**=0.1 T (c) **H**=236.3 A/m, **B**=1.9 T (d) **H**=0.0 A/m, **B**=1.73 T

Fig. 6. Magnetic domain SEM images of the ORIENTCORE HI-B produced by Nippon Steel Co. (100x100 pixels, 0.1 mm/pixel).

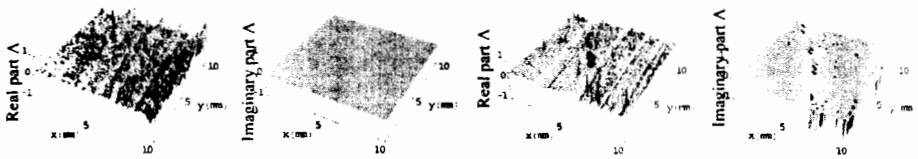

(a) $0.0 \le \mathbf{H} < 2.9$ A/m (b) $2.9 \le \mathbf{H} < 9.3$ A/m

Fig. 7 State transition matrices.

Denoting coercive field $\mathbf{H}_c = \mu_r / \psi$, (16) can be rewritten by

$$\mathbf{H} = \mathbf{H}_c + \mathbf{H}_c = \frac{1}{\mu}\mathbf{B} + \frac{1}{\Psi}\frac{d\mathbf{B}}{d\mathbf{H}} , \tag{23}$$

so that an analytical solution of (23) assuming the constant μ and ψ is given by

$$\mathbf{B} = \mu\mathbf{H} + \varepsilon^{-\frac{\psi}{\mu}\mathbf{H}}\left[\mathbf{B}_0 - \mu\mathbf{H}\right] = \mathbf{B}_f + \varepsilon^{-\frac{\psi}{\mu}\mathbf{H}}\left[\mathbf{B}_0 - \mathbf{B}_f\right] , \tag{24}$$

where $\mathbf{B}_f$, $\mathbf{B}_0$ are the final and initial flux densities, respectively.

Let us consider a characteristic value:

$$\lambda = \frac{\psi}{\mu} \quad [m/A] , \tag{25}$$

then the small and large characteristic values λ correspond to the low and high field regions, respectively. Namely, the small and large λ values reveal the unsaturated and saturated states of the specimen, respectively.

When we have the three magnetic fluxes $\mathbf{B}_i, \mathbf{B}_{i+1}, \mathbf{B}_{i+2}$ as the contrast of SEM images during the field change $\triangle\mathbf{H}$, (24) can be rewritten by

$$\mathbf{B}_{i+1} = \mathbf{B}_{i+2} + \varepsilon^{-\lambda\Delta\mathbf{H}}\left(\mathbf{B}_i - \mathbf{B}_{i+2}\right) . \tag{26}$$

By means of (26), the characteristic value is represented in terms of the SEM images as

$$\lambda = -\frac{1}{\Delta \mathbf{H}} \ln\left[\left(\mathbf{B}_{i+1} - \mathbf{B}_{i+2}\right)^{-1}\left(\mathbf{B}_i - \mathbf{B}_{i+2}\right)\right] \tag{27}$$

Fig. 6 shows the domain images of a grain-oriented electrical steel sheet under the distinct magnetized states. The electrical steel sheet is the ORIENTCORE·HI-B produced by Nippon Steel Corporation and its thickness is 0.23 mm. The observation was carried out using SEM accelerated to 160 kV. Changing the given domain images sequentially by the field excitation, it is easy to visualize the dynamics of magnetic domains. Fig.7 shows the characteristic value distributions determined by (27). Fig. 7(a) suggests the reversible magnetic boundary displacement without pining on the boundary. The real part shown in Fig. 7(b) means the irreversible domain movement. On the other side, the imaginary part shown in Fig. 7(b) can be observed the delay of magnetic boundary displacement at the grain boundary.

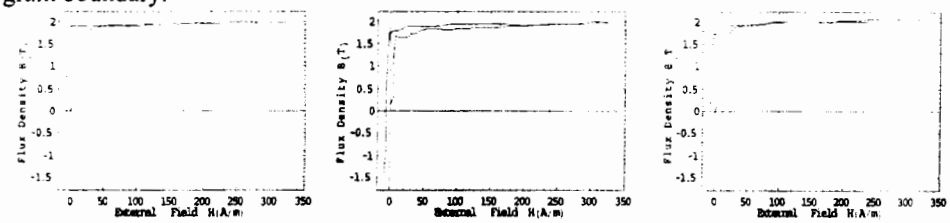

(a) Good crystallized part (b) Lancet part (c) Strained part

Fig. 8. Magnetization characteristics reproduced by (26).

Fig.8 shows the magnetization characteristics curves for which have been reproduced after increasing 111 frames from original 24 frame images by (26) [4].

Thus, by means of IT based model, we have succeeded in obtaining the magnetization characteristics in each of the image pixels on the ferromagnetic materials. This means that the magnetization characteristics can be obtained from the visualized domain images.

3. Conclusion

As shown above, we have derived the magnetization model by means of Fourier series. Assuming the bar-like domain walls has lead to a domain-based model. Further, a composite model by combining the Preisach with domain-based models has been derived. Analytical solution of this composite model leads to the Rayleigh's law. Finally, we have proposed the IT based magnetization model, which can be derived the scanning electron microscopic (SEM, in short) images of the ferromagnetic materials. To demonstrate the capability of this IT based model, we have drawn the magnetization characteristics at the normal, lancet and strained magnetic domains on the SEM image.

References

[1] Y.Saito, S.Hayano, H.Nakamura, Y.Kishino and N.Tsuya, A Representation of Magnetic Hysteresis by Fourier series. Journal of Magnetic Materials 54-57, 1986, pp.1613-1614.

[2] S.Hayano, M.Namiki and Y.Saito, A Magnetization Model for Computational Magneto-dynamics, JAP, 69(8),15 April 1991, pp.4641-4616.

[3] Y.Saito, K.Fukushima, S.Hayano and N.Tsuya, Application of a Chua type Model to the Loss and Skin Effect Calculations, IEEE Trans. Magne., Vol. MAG-23, No. 5, September 1987, pp.2227-2229.

[4] H. Endo, S. Hayano, Y. Saito, and T. L. Kunii, "A Method of Image Processing and Its Application to Magneto-dynamic fields, IEEJ Transaction A, Vol. 120-A, 2000, pp. 913-918.